The $Ni_3Al(111)$ surface structure: experiment and theory

2008 J. Phys.: Condens. Matter 20 195223

(http://iopscience.iop.org/0953-8984/20/19/195223)

J. Phys.: Condens. Matter **20** (2008) 195223 (7pp) doi:10.1088/0953-8984/20/19/195223

The $Ni_3Al(111)$ surface structure: experiment and theory

E Vesselli[1,2], L Bianchettin[1,2], A Baraldi[1,2,5], A Sala[1,2], G Comelli[1,2], S Lizzit[3], L Petaccia[3] and S de Gironcoli[4]

[1] Physics Department and Center of Excellence for Nanostructured Materials, University of Trieste, via A Valerio 2, 34127—Trieste, Italy
[2] Laboratorio Nazionale TASC INFM-CNR, in AREA Science Park, 34012 Trieste, Italy
[3] Sincrotrone Trieste SCpA, SS 14 km 163.5 in AREA Science Park, 34012 Trieste, Italy
[4] SISSA—Scuola Internazionale Superiore di Studi Avanzati and INFM-CNR DEMOCRITOS National Simulation Center, via Beirut 2-4, 34014-Grignano (Trieste), Italy

E-mail: baraldi@elettra.trieste.it

Received 11 January 2008, in final form 18 March 2008
Published 17 April 2008
Online at stacks.iop.org/JPhysCM/20/195223

Abstract
The structure of the $Ni_3Al(111)$ terminal layers has been studied by means of x-ray photoelectron diffraction and density functional theory. The analysis of the diffraction patterns, combined with multiple-scattering simulations, yields structural parameters which are in good agreement with the *ab initio* theoretical results. We find that the first-layer Al atoms move outwards with respect to the Ni atom plane, as previously found by low energy electron diffraction experiments and *ab initio* calculations. The experimentally (theoretically) determined distance between the outermost three layers is reduced by 0.07 ± 0.07 Å (0.06 ± 0.01 Å) and by 0.04 ± 0.08 Å (0.01 ± 0.01 Å) for the first-to-second-layer and second-to-third-layer distances with respect to the bulk value, respectively.

(Some figures in this article are in colour only in the electronic version)

1. Introduction

Most bimetallic alloy surfaces display a significant deviation from the bulk composition in the first three or four atomic layers due to thermodynamic effects. An example is the case of the PtRu and PtRh alloy surfaces [1, 2], where segregation of Pt into the first atomic layer takes place, while substitutional disorder exists in the bulk. In contrast, some of the bimetallic alloys of A_3B type with the $L1_2$ structure, typically referred to as directly ordered alloys, present a bulk-like stoichiometric composition for selected low index crystallographic terminations like the (111) surface, since the mixed terminal layers are energetically favored with respect to pure surfaces. Among them, Ni_3Al, which crystallizes in a face-centered cubic lattice, represents an interesting case because of its applications in electronics, coating technology and for structural elements in engineering systems exposed to high temperatures [3, 4]. Beyond that, NiAl and Ni_3Al surfaces attract remarkable interest as templates for the growth under ultrahigh vacuum (UHV) conditions of thin alumina ordered films [5–8]. Both the structure and the reactivity of these Al oxide layers are widely studied as they constitute UHV model systems of supported catalysts. A first step towards a deep comprehension of the structure and the growth mechanisms of such additional layers is a detailed description of both the structural and the chemical properties of the substrate alloy.

The first structural investigation of the $Ni_3Al(111)$ surface, based on low energy electron diffraction (LEED) [9], reported a bulk-like termination with a small rippled relaxation of the aluminum atoms, each one surrounded by six Ni nearest neighbors in a (2×2) configuration. Al atoms are displaced outwards by 0.06 Å from the Ni plane. Stimulated by theoretical calculations, predicting that a small increase in the stoichiometric 3:1 compositional ratio would result in a pure Ni first layer [10], a recent surface x-ray diffraction (SXRD) study reported an unexpected chemical disorder on the clean surface [11]. The long-range disorder decreases for increasing depth, while the atomic geometrical arrangement is in fair agreement with previous LEED results. This behavior has been explained in terms of chemical disorder at the surface, although

[5] Author to whom any correspondence should be addressed.

the surface is overall stoichiometric. Different conclusions as regards surface order have been reported following scanning tunneling microscopy (STM) measurements [12], revealing a hexagonal array with inter-atomic distances of 4.9 Å, in excellent agreement with the distance between two aluminum nearest neighbors in the (2 × 2) unit cell. In agreement with previous experimental findings, very recent *ab initio* calculations [13] reported an outward shift of the surface Al plane and an inward shift of the Ni plane, resulting in an overall difference of 0.10 Å between the vertical positions of the Al and Ni atoms.

Since the accurate determination of surface lattice relaxation effects is important for a quantitative description of the alloy energetics, we have performed an x-ray photoelectron diffraction (XPD) investigation of the $Ni_3Al(111)$ system. A significant advantage of using XPD with respect to LEED and SXRD techniques is that it is highly sensitive to the local environment of the investigated atom, and does not require a long-range order. Moreover, the forward focusing effect, achieved at high photoelectron kinetic energy, yields a direct identification of the inter-atomic bond directions [14]. The experimental results are complemented by structural calculations based on density functional theory (DFT).

2. Experimental details

Photoelectron diffraction experiments were carried out in a multi-purpose UHV chamber with a base pressure of 5×10^{-11} mbar. The apparatus is equipped with LEED and spot profile analysis LEED optics, a residual gas analyzer for temperature programmed desorption measurements, a Mg Kα x-ray source ($h\nu = 1253.6$ eV $- \Delta E = 0.9$ eV), a monochromatic Al Kα source ($h\nu = 1486.6$ eV $- \Delta E = 0.4$ eV) and a VG MKII hemispherical electron energy analyzer. A five-degree-of-freedom VG Omniax manipulator (three translational axes, polar and azimuthal rotations) is mounted eccentrically on a large differentially pumped rotary flange, so that different instruments, mounted on the radially distributed flanges along the circular chamber perimeter, can be reached. The movement system, the instrument controls and the data acquisition are fully computer driven by custom Labview software. The manipulator allows electron bombardment sample heating up to 1400 K and liquid nitrogen cooling down to 140 K. The $Ni_3Al(111)$ oriented single crystal, acquired from the Surface Preparation Laboratory (SPL), was carefully cleaned by repeated cycles of Ar^+ ion bombardment (2.5 keV) at room temperature and subsequent annealing up to 1175 K. Heating yields surface ordering as well as Al segregation to the outermost layers, which compensates the higher sputtering efficiency for Al versus Ni atoms [11]. Using this procedure a sharp p(2 × 2) LEED pattern, related to the chemical order of the first-surface-layer Ni and Al atoms, was obtained. Surface contaminants such as carbon and sulfur were below the XPS detection limits (<0.01 ML).

The sample crystallographic directions were aligned by means of LEED with respect to the manipulator axis. In figure 1(a) we show the model of the clean surface and define the polar (Θ) and azimuthal (ϕ) angle scales used throughout the work.

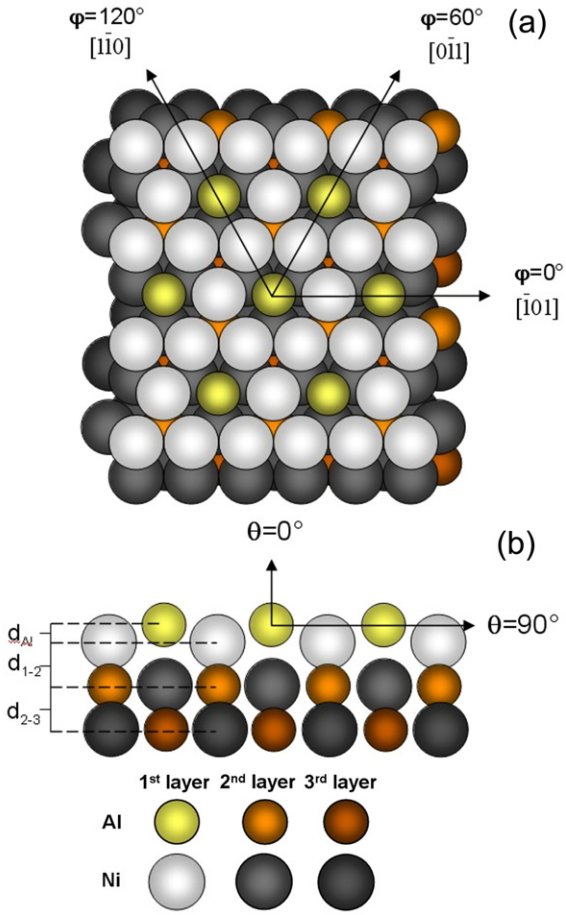

Figure 1. Scheme of the clean $Ni_3Al(111)$ surface structure in top (a) and side (b) views. Al atoms form a p(2 × 2) arrangement in each of the a–b–c stacked layers. Arrows indicate the main crystallographic directions as well as the polar and azimuthal reference angles for the XPD scans.

XPD measurements were acquired using the monochromatic Al Kα radiation, with the sample kept at room temperature. Due to the long measuring time required to collect azimuthal and polar scans needed to yield the full hemispheric mapping, cleaning cycles were regularly alternated with data collection. At each angular position, the Ni $2p_{3/2}$ peak at 852.3 eV binding energy was measured. The photoelectron intensities were obtained by fitting the data with a Doniach–Sunjic [15] function, which accounts for the core-hole lifetime (Lorentzian width) and for the asymmetry of the peaks, convoluted with a Gaussian, related to the thermal, inhomogeneous and experimental broadenings. For each angular scan, the Ni $2p_{3/2}$ intensity was used to calculate the modulation function [13, 15], which is defined as $\chi = (I - I_0)/I_0$. For the azimuthal scans, I_0 is a constant equal to the average intensity. In the case of polar scans, I_0 is instead calculated by data interpolation with a proper cosine function, which accounts for the sampling depth and for the intensity attenuation as a function of the emission angle. For the two-dimensional (2D) stereographic projection of the XPD data, the intensities were normalized in a similar way as a function of the azimuthal and polar angles.

3. Multiple-scattering XPD simulations

The XPD simulations have been performed using the MSCD package developed by Chen and van Hove [16]. The simulation slab was formed by three $Ni_3Al(111)$ planes and a semielliptical cluster of about 270 atoms centered around the chosen emitter. Non-structural parameters such as the Debye temperature and the inner potential were obtained from the literature [9, 17], while the scattering order, cluster size, maximum angular momentum, path-cut, Rehr–Alberts approximation order [18] and finite analyzer acceptance angle were brought to convergence. The inelastic mean free path inside the Ni_3Al alloy was obtained with the TPP-2M formula implemented in the code. All phase shifts and radial matrix elements were calculated by using the PSRM utility program [16].

The overall agreement between simulated and experimental modulation functions was quantified using a multi-spectral reliability factor (R). We adopted the form defined as a normalized summation of the square deviations between the calculated and the experimental χ functions: $R = \sum_i (\chi_{\mathrm{exp},i} - \chi_{\mathrm{sim},i})^2 / \sum_i (\chi^2_{\mathrm{exp},i} + \chi^2_{\mathrm{sim},i})$ [16].

An important point to be discussed is the R-factor analysis which has been performed in order to obtain the best values of the structural parameters. In particular, it is well known that the variability of the R-factor is related to the calculation accuracy and to the possible existence of different relative minima in the R-factor multi-dimensional surface, as a function of both the structural and non-structural parameters. Therefore, a reliability test has been introduced in order to evaluate the accuracy of the results obtained by the comparison between simulation and experiment. For this purpose, we used the quantity var(R) recently introduced [14]. The variance for the minimum value of the R-factor is defined as $\mathrm{var}(R) = R_{\min} \times \sqrt{2/N}$, where N is the number of independent features of structural information present in the data. For example, in an angular scan, N is given by the ratio of the complete angular range divided by the characteristic width of the diffraction modulations [14]. On the basis of this assumption, any structure which is found to have an associated R-factor less than $R_{\min} + \mathrm{var}(R_{\min})$ is regarded as falling within the simulation error bar. On the basis of the above considerations we determined the reliability of our results.

4. DFT calculations

The calculations are based on first-principles density functional theory [19] within the generalized gradient approximation (GGA) [20] for the exchange and correlation (XC) energy functional. The core electrons are represented by ultrasoft pseudopotentials [21] and in order to take into account the effect of magnetism, we performed spin-polarized calculations. The Kohn–Sham equations are solved self-consistently, as implemented in the Quantum-ESPRESSO suite of codes [22]. The Kohn–Sham one-electron orbitals are expanded using plane waves up to a 34 Ryd cutoff energy. In order to deal with the metallic character of the system, the k-space integrations over the Brillouin zone (BZ) are performed using a $(12 \times 12 \times 12)$ Monkhorst–Pack [23] mesh, where each k-point contribution is broadened by a Methfessel and Paxton [24] smearing function of order 1 with a width of 0.012 Ryd.

Ni_3Al crystallizes in the cubic $L1_2$-type structure with Al atoms at the cubic corners and Ni atoms at the face center positions [25]. From bulk calculations we obtain an equilibrium lattice constant of 3.57 Å which is equal to the experimental value [26].

We model the surface with a (2×2) unit cell and seven-layer repeated slabs with a vacuum region of 10 Å in order to make the inter-slab interactions negligible. Both sides and all layers are relaxed except the central layer of the slab.

Ionic forces are the energy derivative with respect to the ions displacement. On the basis of this, the geometry was optimized until all components of ionic forces on each atom were smaller than 0.001 Ryd Bohr^{-1} and the total energy variation less than 10^{-6} Ryd. The numerical accuracy of the structural parameters thus obtained can be estimated to be less than 0.005 Bohr from the residual forces and bond stiffnesses, as estimated from vibrational frequencies. The inaccuracy associated with the approximate treatment of exchange and correlation is difficult to quantify but since structural properties are usually rather insensitive to details in the XC functional we estimate that the overall uncertainty of the theoretical structural parameters is below 0.01 Å.

5. Results

In order to obtain the structural parameters of the $Ni_3Al(111)$ surface, we initially performed azimuthal and polar scans along selected directions. In figures 2 and 3, the experimental χ functions are plotted together with the corresponding best R-factor multi-scattering simulation results. The best structural parameters have been obtained by comparing experimental and computed χ functions according to the following procedure. As a first step we set the structural parameters to the bulk Ni_3Al values and optimized the non-structural degrees of freedom. Consequently, we also let the structure of the slab vary. On the basis of previous findings [11, 27], the nearest-neighbor distance within a single (111) plane was assumed to be 2.52 Å, then the distances between the outermost three atomic layers were varied minimizing the R-factor. Finally, the first-layer Al atoms were allowed to move outwards. In our calculations we did not consider antisite substitutional defect configurations (Ni or Al) and we always used a nominally $3_{\mathrm{Ni}}{:}1_{\mathrm{Al}}$ stoichiometric structure. Since the displacement of the Al atoms in the second and deeper layers with respect to Ni atoms in the same planes did not yield appreciable variation of the R-factor, we did not include this degree of freedom in the optimization of the structural parameters. In figure 4 we plot the results of this optimization. In the upper panel (figure 4(a)), the R-factor behavior as a function of the distance between the first Al and Ni layers is depicted. In the bottom panel (b), the 2D contour plot describes the R-factor behavior as a function of the relaxation/contraction of the first two inter-layer distances with respect to the bulk value. From this analysis, we get a minimum R-factor of 0.2275, which is obtained

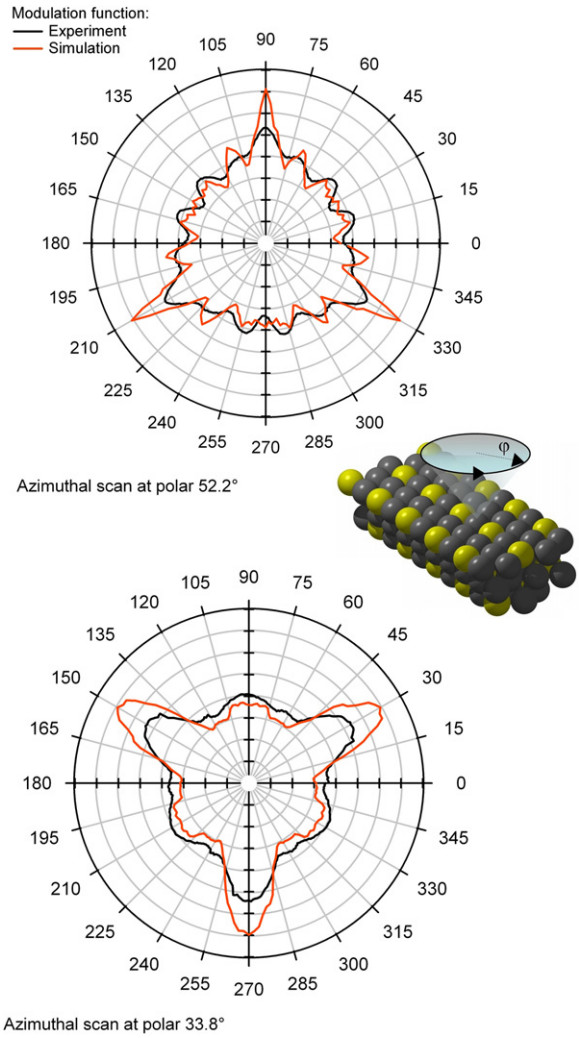

Figure 2. Plots of the modulation function of selected experimental and calculated azimuthal scans. A structural model is also shown in order to define the scanning angles. The azimuth was varied experimentally within a 120° span and data were subsequently replicated.

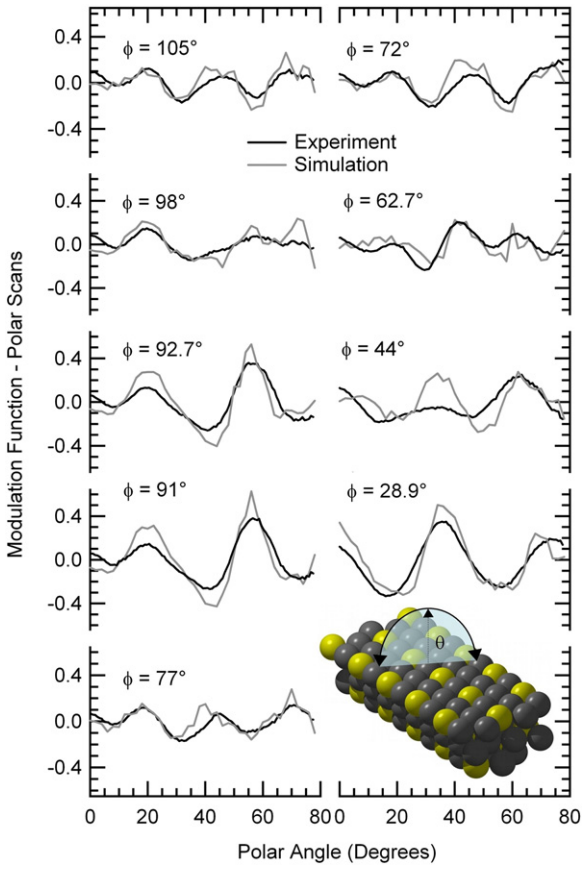

Figure 3. Plots of modulation functions of selected experimental and calculated polar scans. A structural model is also shown in order to define the scanning angles.

upon grid sampling of the three-dimensional space (d_{12}; d_{23}; d_{Al}) after optimization of the non-structural parameters. On the basis of the criterion described in section 3, the *R*-factor variance is 0.03. This value has been obtained by considering a total sampled angular range of about 1000° (measured polar scans spanned 80°, while azimuthal scans spanned 120°) and a characteristic feature width of 7°, determined as a best fit value of the angular resolution of the electron energy analyzer. Even though the angular width of the main features is often intrinsic and not related only to the acceptance angle of the analyzer, this value is often used as an adjustable parameter in the calculations, in order to compensate for other contributions, such as the mean free path determination, which cannot always be properly evaluated. The structure with this best *R*-factor shows that the two terminal planes are slightly contracted with respect to the bulk value of 2.055 Å [9]. Indeed, we find $d_{12} = 1.99 \pm 0.07$ Å and $d_{23} = 2.01 \pm 0.08$ Å, corresponding to contractions of 3% and 2%, respectively. The *R*-factor analysis suggests also that an extrusion of the surface Al atoms (d_{Al}) of 0.15 Å is present. This result is however only indicative, since the associated error bar is of the order of 0.3 Å, estimated on the basis of a parabolic fit of the *R*-factor trend as a function of d_{Al}.

The upper panel of figure 5 shows the stereographic projection of the experimental mapping of the Ni $2p_{3/2}$ photoemission intensity. The experimental data were limited to the angular range 0°–80° for θ, and 12°–132° for φ, and then replicated to plot the full projection. We have simulated with the MSCD package the intensity in the full hemisphere, using the structural parameters previously determined with the *R*-factor minimization. The result of this calculation, displayed in figure 5(b) as stereographic projection, shows a remarkable agreement with the experimental data of figure 5(a).

The structural parameters that we obtain from our DFT calculations are in very good agreement with the experimental findings as shown in table 1. We obtain a first-layer buckling with Al atoms displaced by 0.08 Å over the plane of Ni atoms. The Ni–Ni first-to-second-layer distance results as 2.00 Å, i.e. 2.9% contracted with respect to the bulk value of 2.06 Å; the second-layer Al atoms are 0.02 Å inward displaced with respect to the Ni atoms of the same layer, resulting in an Al–Al first-to-second-layer distance of 2.11 Å (+2.4%). In the third layer the Al atoms result as coplanar with the Ni atoms and the second-to-third-inter-layer spacing (Ni–Ni distance of

Table 1. Comparison of our results (experimental and theoretical) with the literature data for the structural relaxations of the $Ni_3Al(111)$ surface layers.

	XPD (present work)	DFT (present work)	Literature	Ref.
d_{Al}	$+0.15^b$	$+0.08$	$+0.06 \pm 0.03$	[9]
			$+0.02 \pm 0.01$	[11]
			$+0.10$	[13]
$d_{1-2} - d_0$ (relaxation)	-0.07 ± 0.07	-0.06	-0.01 ± 0.03	[9]
			-0.02 ± 0.01^a	[11]
			-0.08^a	[13]
$d_{2-3} - d_0$ (relaxation)	-0.04 ± 0.08	-0.01	-0.04 ± 0.01^a	[11]
			-0.04^a	[13]

[a] Values indicated by an asterisk refer to the mean positions of the Al and Ni atoms within a given layer, as reported in [11] and [13]. Inter-layer relaxation values are reported with respect to the bulk value $d_0 = 2.055$ Å.

[b] Due to the reliability associated with the R-factor analysis, we quote this value as an estimate only: see the text for details.

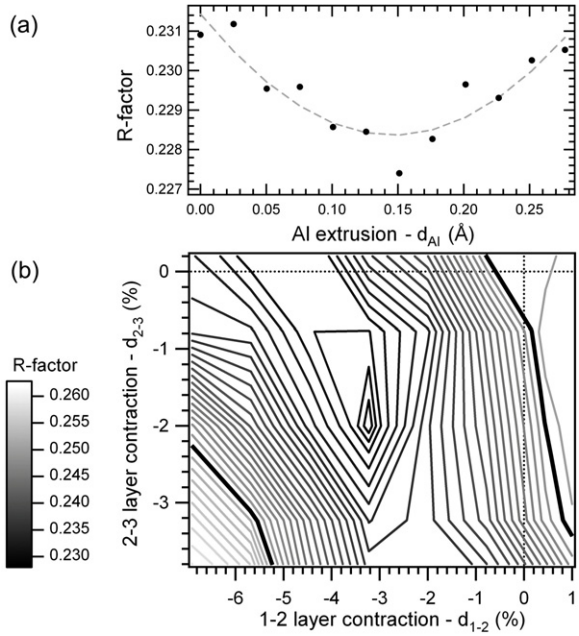

Figure 4. Plots of the R-factor as a function of the examined structural parameters: (a) R-factor versus first-layer Al atom extrusion, (b) R-factor versus d_{12} and d_{23} distances. The d_{12} distance is calculated with respect to the first-layer Ni plane. The bold line indicates the R-factor confidence perimeter. See the text for further details.

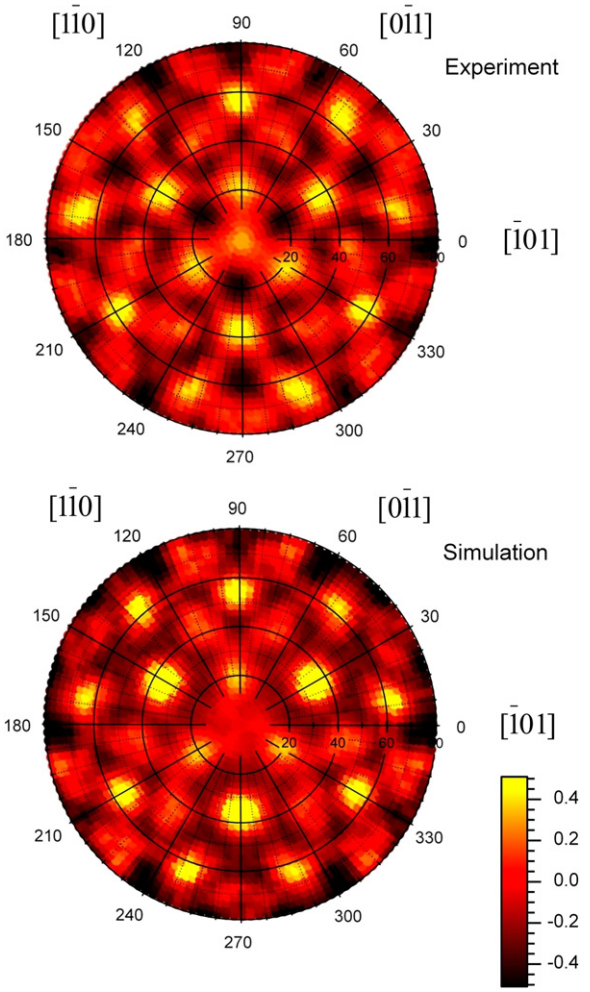

Figure 5. Experimental (top) and calculated (bottom) 2D stereographic plots of the Ni $2p_{3/2}$ intensity as a function of the polar (0–80°) and azimuthal (0–360°) coordinates. The main crystallographic directions are also shown.

2.05 Å) results as contracted by only 0.4%. All the results are also in agreement with the most recent theoretical work on this surface [13].

6. Discussion

Our experimental and theoretical results are in good agreement with previous studies that find an outward displacement of the terminal layer Al atoms with respect to the first-layer Ni atoms, which are in contrast inward contracted with respect to the bulk inter-layer distance (see table 1). However, we get a larger contraction of the first-to-second-layer distance with respect to the previously published LEED and SXRD results [9, 11], while our estimate is in agreement with the most recent DFT calculations [13]. For the experimental techniques, the origin

of this discrepancy could be due to the fact that both LEED and SXRD yield information which is obtained by diffraction processes in long-range ordered structures. In contrast, in XPD the diffraction process is local, the reference wave being generated by an emitter atom in the sample. For this reason, the chemical disorder present on the alloy termination, which has been evidenced both by XRD and STM [11, 12], clearly affects in a different way the results obtained with the above techniques.

The agreement between simulated and experimental structures is good and the best R-factor obtained is quite low; nevertheless, a better R-factor might have been obtained by using a cluster of larger size, in order to allow for more than three Ni_3Al layers in the trial structures. This goes beyond the MSCD code capabilities due to the exceedingly large number of inequivalent atoms required. Due to the absence of a repetition of equivalent layers in the simulation (since a single a–b–c stacking has been introduced) the forward scattering peak at ($\theta = 0$), present in the experimental results of figure 5(a), has a very low intensity in the simulated 2D stereographic plot data.

By comparing the experimental and simulated χ functions reported in figures 2 and 3, it can be observed that the positions of the diffraction peaks are well reproduced by the calculation, while the modulation intensities are slightly amplified with respect to the measured data. In the azimuthal scan plots we have shown the normalized χ function, in which the simulated diffraction modulation amplitudes are scaled to fit the experimental data, so that the agreement in angular position of the structures is highlighted. In contrast, in figure 3 we have plotted the absolute χ function for the polar scans, so that the discrepancy between the amplitudes of the modulations is evident.

The above considerations about the reliability of the R-factor analysis (see previous sections) are essential in the case of the buckling effect of the Al atoms, where the poor sensitivity of the high kinetic energy photoemitted electrons to the low Al scattering cross section corresponds only to minor changes in the modulation functions when the Al atomic positions are changed, yielding R-factor variations well beyond the attainable accuracy. Despite this, the d_{Al} value which minimizes the R-factor combines with our DFT calculations, which unambiguously show the outward Al displacement in the first layer, in agreement with analogous results obtained by DFT calculations for the same system that recently appeared in the literature [13].

This seems to be a general rule for $L1_2$–$A_3B(111)$ surfaces. Indeed it has been suggested [28] that the $L1_2$–A_3B alloy lattice constant should be comparable to the weighted average of pure A and B single-crystal bulk lattice parameters. Moreover, if the higher concentration A element is characterized in the pure substance by a smaller lattice constant with respect to the pure B single crystal, the mismatch in the alloy is expected to generate a surface strain inducing an outward displacement of the B element. In the case of Ni_3Al, the pure Al lattice parameter (4.049 Å) [29] is about 15% larger than that of the pure Ni crystal (3.524 Å) [29] and, indeed we find an Al outward buckling in the relaxed structure. That same behavior characterizes also other $L1_2$–$A_3B(111)$ surfaces like Cu_3Pd and Cu_3Au [30] where the outward bucklings result as 0.1 Å and 0.17 Å, respectively. LEED experiments have shown that also for the $Pt_3Sn(111)$ surface [31] Sn atoms are outward relaxed by 0.21 Å, even though the comparison with the previous systems is not immediate because the pure Sn does not crystallize in face-centered cubic but in a tetragonal geometry.

7. Conclusions

We investigated the structure of the $Ni_3Al(111)$ surface by means of photoelectron diffraction of the Ni $2p_{3/2}$ core level excited by Al Kα radiation, combined with multiple-scattering simulation of the photoemission intensity. Our experimental findings are corroborated by DFT calculations. The two approaches agree with previous results in confirming a contraction of the terminal inter-layer distances, accompanied by an outward relaxation of the first-layer Al atoms with respect to the Ni atoms.

Acknowledgments

We gratefully thank C Scozzari for writing key parts of the data acquisition software, F Bondino and A Verdini for helpful discussions about the MSCD code suite. We acknowledge financial support from Sincrotrone Trieste SCpA.

References

[1] Yuge K, Seke A, Kuwabara A, Oba F and Tanaka I 2006 *Phys. Rev.* B **74** 174202
van Delft F C M J M and Nieuwenhuys B E 1986 *Surf. Sci.* **178** 880
[2] Ruban A V, Skriver H L and Nørskov J K 1999 *Phys. Rev.* B **59** 15990
[3] Lu Y, Chen W and Eadie R 2004 *Intermetallics* **12** 1299
[4] Stoloff N S, Liu C T and Devvi S C 2000 *Intermetallics* **8** 1313
[5] Kresse G, Schmid M, Napetsching E, Shishkin M, Köhler L and Varga P 2005 *Science* **308** 1440
Stierle A, Renner F, Streitel R, Dosch H, Drube W and Cowie B C 2004 *Science* **303** 1652
[6] Gritschneder S, Becker C, Wandelt K and Reichling M 2007 *J. Am. Chem. Soc.* **129** 4925
[7] Ceballos G, Song Z, Pascual J I, Rust H P, Conrad H, Bäumer M and Freund H J 2002 *Chem. Phys. Lett.* **359** 41
[8] Hamm G, Barth C, Becker C, Wandelt K and Henry C R 2006 *Phys. Rev. Lett.* **97** 126106
[9] Sondericker D, Jona F and Marcus P M 1986 *Phys. Rev.* B **34** 6770
[10] Ruban A V 2002 *Phys. Rev.* B **65** 174201
[11] Bikondoa O, Castro G R, Torrelles X, Wendler F and Moritz W 2005 *Phys. Rev.* B **72** 195430
[12] Addepalli S G, Ekstrom B, Magtoto N P, Lin J S and Kelber J A 1999 *Surf. Sci.* **442** 385
[13] Jurczyszyn L, Krupski A, Degen S, Pieczyrak B, Kralj M, Becker C and Wandelt K 2007 *Phys. Rev.* B **76** 45101
[14] Woodruff D P 2007 *Surf. Sci. Rep.* **62** 1
[15] Doniach S and Sunjic M 1970 *J. Phys. C: Solid State Phys.* **3** 185
[16] Chen Y and van Hove M A MSCD code, http://www.sitp.lbl.gov/index.php?content=/mscdpack/mscdpack.html
[17] Stassis C, Kayser F X, Loong C K and Arch D 1981 *Phys. Rev.* B **24** 3048

[18] Chen Y, García de Abajo F J, Chassé A, Ynzunza R X, Kaduwela A P, van Hove M A and Fadley C S 1998 *Phys. Rev.* B **58** 13121
[19] Hohenberg P and Kohn W 1964 *Phys. Rev.* **136** B864 Kohn W and Sham L 1965 *Phys. Rev.* **140** A1133
[20] Perdew J P, Burke K and Ernzerhof M 1996 *Phys. Rev. Lett.* **77** 3865
[21] Vanderbilt D 1990 *Phys. Rev.* B **41** 7892
[22] Baroni S, de Gironcoli S, Dal Corso A and Giannozzi P http://www.quantum-espresso.org
[23] Monkhorst H J and Pack J D 1976 *Phys. Rev.* B **13** 5188
[24] Methfessel M and Paxton A T 1989 *Phys. Rev.* B **40** 3616
[25] Xu J H, Min B I, Freeman A J and Oguchi T 1990 *Phys. Rev.* B **41** 5010
[26] Mohan Rao P V, Suryanarayana S V, Satyanarayana Murthy K and Nagender Naidu S V 1989 *J. Phys.: Condens. Matter* **1** 5357
[27] Jurczyszyn L, Rosenhahn A, Schneider J, Becker C and Wandelt K 2003 *Phys. Rev.* B **68** 115425
[28] Jacob T and Goddard W A 2000 4 *J. Phys. Chem.* B **108** 8311
[29] http://www.webelements.com/
[30] Bozzolo G, Garces J E, Noebe R D, Abel P and Mosca H O 2003 *Prog. Surf. Sci.* **73** 79
[31] Atrei A, Bardi U, Rovida G, Torrini M, Zanazzi E and Ross P N 1992 *Phys. Rev.* B **46** 1649